



HAL
open science

Manipulating the Relaxation of Quasi-D4d Dysprosium Compounds through Alternation of the O-Donor Ligands

Mei Guo, Jianfeng Wu, Olivier Cador, Jingjing Lu, Bing Yin, Boris Le Guennic, Jinkui Tang

► **To cite this version:**

Mei Guo, Jianfeng Wu, Olivier Cador, Jingjing Lu, Bing Yin, et al.. Manipulating the Relaxation of Quasi-D4d Dysprosium Compounds through Alternation of the O-Donor Ligands. *Inorganic Chemistry*, 2018, 57 (8), pp.4534-4542. 10.1021/acs.inorgchem.8b00294 . hal-01771520

HAL Id: hal-01771520

<https://univ-rennes.hal.science/hal-01771520v1>

Submitted on 20 Jun 2018

HAL is a multi-disciplinary open access archive for the deposit and dissemination of scientific research documents, whether they are published or not. The documents may come from teaching and research institutions in France or abroad, or from public or private research centers.

L'archive ouverte pluridisciplinaire **HAL**, est destinée au dépôt et à la diffusion de documents scientifiques de niveau recherche, publiés ou non, émanant des établissements d'enseignement et de recherche français ou étrangers, des laboratoires publics ou privés.

Manipulating the Relaxation of Quasi- D_{4d} Dysprosium Compounds through Alternation of the O-donor Ligands

Mei Guo,^{†, §} Jianfeng Wu,^{†, ||} Olivier Cador,[‡] Jingjing Lu,[†] Bing Yin,^{*, ‡} Boris Le Guennic^{*, ‡} and Jinkui Tang^{*, †}

[†]State Key Laboratory of Rare Earth Resource Utilization, Changchun Institute of Applied Chemistry, Chinese Academy of Sciences, Changchun 130022, P. R. China

[‡]Key Laboratory of Synthetic and Natural Functional Molecule Chemistry of Ministry of Education, College of Chemistry and Materials Science, Northwest University, Xi'an, 710069, P. R. China

[§]University of Chinese Academy of Sciences, Beijing, 100049, P. R. China

^{||}Sino-German Joint Research Lab for Space Biomaterials and Translational Technology, School of Life Sciences, Northwestern Polytechnical University, Xi'an, 710072, P. R. China

[‡]Univ Rennes, CNRS, ISCR (Institut des Sciences Chimiques de Rennes) - UMR 6226, F-35000 Rennes, France

ABSTRACT: Three mononuclear Dy^{III} complexes with the same auxiliary ligand Lz (2,4-diamino-6-pyridyl-1,3,5-triazine), [Dy(TTA)₃Lz] (**1Dy**) (TTA = 4,4,4-trifluoro-1-(2-thienyl)-1,3-butanedionate), [Dy(acac)₃Lz]·CH₃OH·0.5H₂O (**2Dy**) (acac = acetylacetonate), and [Dy(MQ)₂Lz₂]Br·CH₃OH (**3Dy**) (HMQ = 2-methyl-8-quinolinol), have been synthesized through alteration of the ligands containing O donors. In all three complexes, the Dy^{III} ions are eight-coordinate and submitted to pseudo- D_{4d} symmetry in the first coordination sphere. It is noteworthy that the TTA ligands in **1Dy** are easily substituted by other bidentate capping ligands with O donors, leading to distinct magnetic properties, which were studied experimentally and via *ab initio* calculations. All three complexes were found to exhibit single-molecule magnets behavior with U_{eff} of 22 cm⁻¹ (**1Dy**), 112 cm⁻¹ (**2Dy**), and 56 cm⁻¹ (**3Dy**) under zero applied dc field. Complex **1Dy** demonstrates inferior SIM properties compared with **2Dy** and **3Dy**, which can be attributed to the strong electron-withdrawing effects of TTA ligands, as confirmed by theoretical calculations. However, butterfly-shaped magnetic hysteresis in **1Dy** and **3Dy** were observed at 1.9 K, while not in **2Dy**.

INTRODUCTION

Single-ion magnets (SIMs) with only one spin centre within a molecule have flourished as an important class of single-molecule magnets (SMMs) in recent years.¹ Contrary to transition-metal single-ion magnets,² such as the linear [Fe(C(SiMe₃)₃)₂]⁻ showing energy barrier of 226 cm⁻¹ (325 K) in a zero applied dc field,³ lanthanide-based single-ion magnets^{1c, 4} with strong internal single-ion anisotropy, especially those complexes containing Dy^{III}, Tb^{III} and Er^{III} ions, demonstrate great potential in enhancing SMM properties. Remarkably, a dysprosium metallocenium cation [(Cp^{III})₂Dy]⁺ (Cp^{III} = 1,2,4-tri(tert-butyl)cyclopentadienide) SIM exhibits a record blocking temperature, T_B up to 60 K.⁵ Two versions of the anisotropy barrier are 1277 cm⁻¹ (1837 K)^{5a} and 1223 cm⁻¹ (1760 K),^{5b} which are comparable to that of the [Dy(O^tBu)₂(py)₃][BPh₄] complex (1261 cm⁻¹, 1815 K).^{4b}

For the great majority of lanthanide-based SMMs, QTM relaxation behavior occurs under zero-dc applied field, especially in SIMs.⁶ Considering that the fast QTM will shortcut the Orbach relaxation process in the low-temperature region, reducing the anisotropy barriers (U_{eff}), therefore the suppression of QTM is a crucial issue for realizing the application of spin-based devices.⁷ Up to now, among the methods adopted to suppress QTM as efficiently as possible, one can cite the modulation of ligand field to obtain an ideal axial symmetry,⁸ applying a dc magnetic field,^{6c, 9} magnetic dilution¹⁰ or isotopic enrichment¹¹. For dinuclear and multinuclear lanthanide SMMs, strong magnetic exchange

coupling between the spin centers can hinder zero-field fast relaxation pathway,¹² while for mononuclear lanthanide SMMs, high symmetry systems, such as D_{4d} ¹³ and D_{5h} ^{4b}, have been widely investigated, in which the vanishing off-diagonal crystal field parameters B_k^q ($q \neq 0$) can control the mixing m_J levels.¹⁴

Lanthanide β -diketone complexes with quasi square antiprismatic (SAP) geometry (D_{4d}) behave as promising systems to design high anisotropy barrier SIMs.¹⁵ The first significant development of this kind of complexes was reported by Gao *et al.*, where the complex [Dy(acac)₃(H₂O)₂] showed a typical SIM behavior.^{6c} When the two H₂O molecules in the complex [Dy(acac)₃(H₂O)₂] were replaced by diverse auxiliary ligands, such as 1,10-phenanthroline (phen) and its large aromatic derivatives, the properties of the corresponding SIMs have changed obviously.¹⁶ In addition to the β -diketone ligand, the nitrogen-enriched ligand Lz¹⁷ was used as co-ligands to construct SMMs with D_{4d} symmetry and better magnetic properties. Among the D_{4d} symmetry Dy-based SMMs reported to date, [DyLz₂(*o*-vanillin)₂]·NO₃·solvent complex represents the most successful example that enhances the anisotropy barrier (U_{eff} = 615 K) and the hysteresis loop (T_B = 7 K), which can be attributed to strong axial anisotropy resulted from the rotation of the plane of the square-antiprismatic geometry.¹³

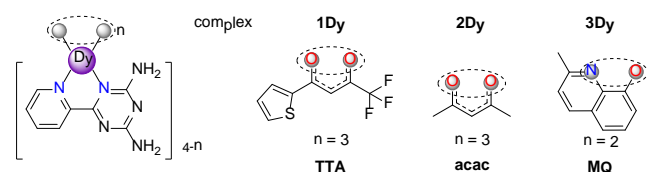
According to the above studies, we synthesized three new complexes based on the Lz ligand, i.e. [Dy(TTA)₃Lz] (**1Dy**), [Dy(acac)₃Lz]·CH₃OH·0.5H₂O (**2Dy**), and [Dy(MQ)₂Lz₂]Br·CH₃OH (**3Dy**). The Dy^{III} centers in all three

complexes adopt the eight-coordinated N_xO_{8-x} coordination environment showing the distorted D_{4d} local symmetry. Contrary to previous studies, herein, we investigate the relaxation dynamics of three dysprosium complexes with quasi- D_{4d} coordination symmetry through fixing the N-containing ligands while modification of the ligands containing O donors (Scheme 1). In these complexes, the effective energy barrier varies remarkably due to change of the ligands containing O donors. Magneto-structural studies and theoretical calculations reveal that the alternation of the O-donor ligands induces significant impact on the Dy-based single-ion magnets.

EXPERIMENTAL SECTION

Materials and Methods. The ligand Lz was synthesized by the literature procedure previously published.¹⁸ Other materials were commercially available and used as received without further purification. IR spectra were obtained using a Nicolet 6700 Flex FTIR spectrometer with ART module in the range from 500 to 4000 cm^{-1} . Elemental analysis for C, N and H were performed *via* a Perkin-Elmer 2400 analyzer.

Scheme 1. Schematic structures of compounds **1Dy**, **2Dy** and **3Dy**.



Synthesis of [Dy(TTA)₃Lz] (1Dy). Dy(TTA)₃·2H₂O (0.1 mmol) was added to a solution of Lz (0.1 mmol) in mixture of MeOH/CH₂Cl₂ (5 mL/10 mL). The solution was stirred for 4 h, and the filtrate was left unperturbed to allow to crystallize by slow evaporation. Colorless crystals of **1Dy** were obtained after few days. Yield: ~60%. Selected IR (cm^{-1}): 3327 (w), 3208 (br), 1597 (s), 1579 (s), 1538 (s), 1458 (m), 1409 (m), 1352 (m), 1300 (s), 1250 (s), 1181 (s), 1128 (s), 1061 (m), 1015 (m), 934 (m), 856 (m), 788 (w), 768 (w), 719 (m), 682 (m), 640 (s), 579 (m).

Synthesis of [Dy(acac)₃Lz]·CH₃OH·0.5H₂O (2Dy). Dy(acac)₃·2H₂O (0.2 mmol) was added to a solution of Lz (0.2 mmol) in mixture of MeOH/CH₂Cl₂ (10 mL/5 mL), and then trimethylamine (0.2 mmol) was added. The solution was stirred for 4 h, and the filtrate was allowed to crystallize by slow evaporation. Colorless crystals of **2Dy** were obtained after few days. Yield: ~55%. Selected IR (cm^{-1}): 3615 (w), 3329 (m), 3213 (m), 1578 (s), 1556 (m), 1513 (s), 1455 (m), 1393 (s), 1262 (s), 1190 (w), 1012 (s), 921 (m), 797 (m), 655 (w). Anal. Calcd. for [Dy(acac)₃Lz]·CH₃OH·0.5H₂O (C₄₈H₆₈Dy₂N₁₂O₁₅, MW = 1378.14): C, 41.83%; H, 4.97%; N, 12.19%. Found: C, 42.01%; H, 4.89%; N, 12.32%.

Synthesis of [Dy(MQ)₂Lz₂]Br·CH₃OH (3Dy). DyBr₃·H₂O (0.1 mmol) was added to a solution of Lz (0.2 mmol) and HMQ (0.2 mmol) in mixture of MeOH/CH₂Cl₂ (10 mL/5 mL), and then trimethylamine (0.1 mmol) was added. The solution was stirred for 4 h, and the filtrate was allowed to crystallize by slow evaporation. Yellow crystals of **3Dy** were obtained after few days. Yield: ~40%. Selected IR (cm^{-1}): 3288 (w), 3103 (br), 1660 (m), 1584 (w), 1557 (m), 1501 (m), 1450 (m), 1394 (w), 1373 (w), 1326 (s), 1305(w), 1270 (m), 1196 (w), 1101 (m), 1054 (w), 1012 (m), 986 (w), 869 (w), 788 (s), 741 (vs), 702 (m), 637 (s), 553 (w). Anal. Calcd. for

[Dy(MQ)₂Lz₂]Br·CH₃OH (C₃₇H₃₆BrDyN₁₄O₃, MW = 967.21): C, 45.94%; H, 3.75%; N, 20.27%. Found: C, 46.02%; H, 3.77%; N, 20.34%.

X-ray Crystallography. Crystallographic data of three complexes were collected using a Bruker Apex II CCD diffractometer equipped with graphite-monochromatized Mo-K α radiation ($\lambda = 0.71073 \text{ \AA}$). Data processing was accomplished with the SAINT processing program. The structures were solved by direct methods and refined by full-matrix least-squares methods on F^2 using SHELXTL-2014.¹⁹ All non-hydrogen atoms were refined anisotropically. The H atoms were introduced in calculated positions and refined with fixed geometry with respect to their carrier atoms. In **2Dy**, the hydrogen atoms of the water solvent (O15) were not modelled and the hydrogen atoms have been placed on a disordered O atom (O13). The solvent accessible VOIDS in **3Dy** are due to a large amount of disordered solvents in this structure.

Magnetic Measurements. Magnetic susceptibility measurements were recorded on a Quantum Design MPMS-XL7 SQUID magnetometer equipped with a 7 T magnet. Direct-current (dc) measurements were collected with an external magnetic field of 1 kOe in the temperature range of 1.9–300 K. The alternating-current (ac) measurements were investigated in a 3.0 Oe ac oscillating field with frequencies between 1 and 1500 Hz. The experimental magnetic susceptibility data for all compounds were corrected for diamagnetic contributions estimated using Pascal's constants.²⁰

Computational details. *Ab initio* calculations based on multi-configurational wavefunction method and spin-orbit coupling (SOC)²¹ were performed on the experimental structures of **1–3Dy** to rationalize their magnetic properties. At first, a set of spin eigenstates of different multiplicities are obtained by the CASSCF²² method. Then the SOC matrix in the space spanned by these spin eigenstates are further diagonalized²¹ to obtain various Kramers doublets (KD). In the CASSCF step, the active space, consisted of 9 electrons in 7 orbitals, is utilized to obtain the wavefunctions of 21 spin sextets, 224 quartets as well as 490 doublets. In the step of the diagonalization of the SOC matrix,²³ only 21 sextets, 128 quartets and 98 doublet states were included due to the hardware limitations. The ANO-RCC basis sets²⁴ were used with Dy described by VTZP, O and N described by VDZP as well as other atoms described by VDZ. The g -tensors and other parameters describing the magnetic anisotropy of the low-lying KDs were obtained according to the procedure by Chibotaru *et al.*²⁵ All the calculations were carried out with the MOLCAS@UU code, a freely distributed version of MOLCAS 8.0 program.²⁶

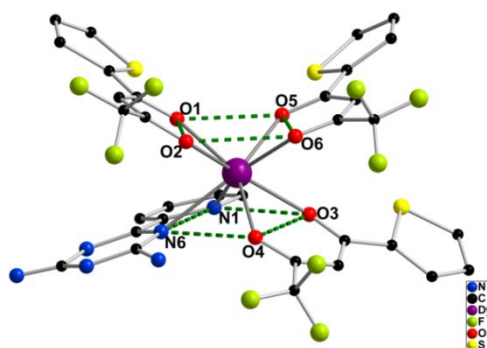


Figure 1. Molecular structure of **1Dy**. H atoms are omitted for clarity.

RESULTS AND DISCUSSION

Crystallography. Single-crystal X-ray diffraction investigation revealed that **1Dy** (Figures 1 and 2) and **2Dy** (Figure 3) crystallize in the monoclinic $P2_1/c$ space group with $Z = 4$, whereas complex **3Dy** (Figures 4 and S1) crystallizes in the triclinic $P\bar{1}$ space group with $Z = 2$. Details of the crystallographic data and the structure solution are summarized in Table S1, whereas selected bond distances and angles are listed in Table S2. The complexes **1Dy** and **2Dy** were isolated through the change of the coordinated water molecules of $[\text{Dy}(\text{TTA})_3 \cdot 2\text{H}_2\text{O}]$ and $[\text{Dy}(\text{acac})_3 \cdot 2\text{H}_2\text{O}]$ by changing ligand Lz.

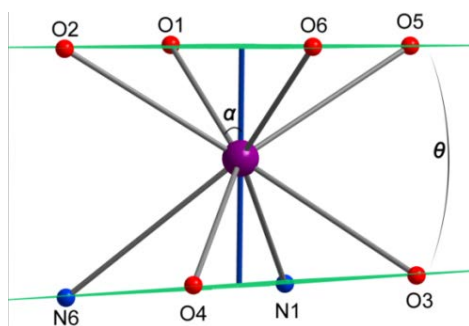


Figure 2. Angle α between the S_8 axis and a Dy–L vector, and angle θ between the upper and lower coordination planes of complex **1Dy**.

The asymmetric unit of **1Dy** consists of one Dy^{III} ion, three TTA ligands providing six O-donor atoms, and one ligand Lz with two N atoms coordinated to Dy^{III} ion, giving rise to a distorted square-antiprismatic geometry. The unit cell of **2Dy** contains two crystallographically independent molecules, **2Dy^a** and **2Dy^b** (Figure 3). The Dy^{III} ions of complex **2Dy** are in the same N_2O_6 square-antiprismatic coordination environment with two N atoms from the one Lz ligand and six O atoms from the three acac ligands. The basal planes are constructed by atoms O1, O2, O5, O6 and N1, N6, O4, O3 for **1Dy** (Figure 1), and O1, O2, O5, O6 and O3, O4, N1, N2 for **2Dy^a**, and O9, O10, O11, O12 and O7, O8, N3, N4 for **2Dy^b** (Figure 3). The analysis of the exact geometry of complexes by using the *SHAPE* 2.1 software²⁷ reveals that all Dy^{III} ions reside in the square-antiprismatic coordination geometry (D_{4d}) with *CshMs* (the Continuous Shape Measures values) of 0.572, 0.906, 0.828 for **1Dy**, **2Dy^a** and **2Dy^b**, respectively (Table S3). The Dy–O distances range from 2.301(7) to 2.346(7), 2.300(3) to 2.346(3), and 2.308(8) to 2.326(4) Å; while the average Dy–N distances of 2.553(5), 2.596(9), and 2.583(9) Å for **1Dy**, **2Dy^a** and **2Dy^b**, respectively (Table S2). The angles between the pseudo S_8 axis and the Dy–L direction (Figure 2), α (54.74° for the ideal α value), vary from 57.5° to 60.5° , 56.5° to 62.5° , and 56.8° to 58.7° for **1Dy**, **2Dy^a** and **2Dy^b**, respectively, indicating an axial compression of the coordinating environment in all three crystal structures.²⁸ Besides, the θ angle (Figure 2) between two basal planes is 3.3° , 2.4° , and 4.4° for **1Dy**, **2Dy^a** and **2Dy^b**, respectively. The shortest intermolecular Dy...Dy distance is 8.02 Å for **1Dy**, suggesting the

possible existence of intermolecular interactions. The distance between the **Dy1** and **Dy2** is 10.57 Å in complex **2Dy**, which does not necessarily preclude any intermolecular exchange interactions.

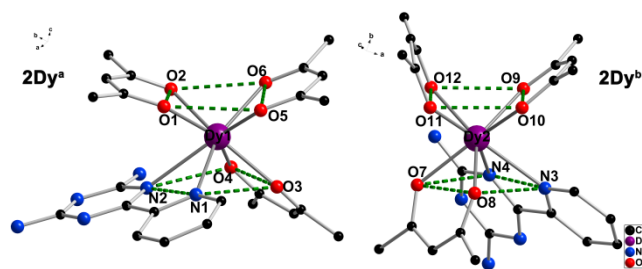


Figure 3. Molecular structures of **2Dy^a** (left) and **2Dy^b** (right). H atoms and solvent molecules are omitted for clarity.

For complex **3Dy**, the Dy^{III} ion is in a N_6O_2 square-antiprismatic coordination geometry with two N atoms and two O atoms from the two 2-methyl-8-quinolinol ligands, and four N atoms from the two Lz ligands. Complex **3Dy** is further charge balanced by an anion Br^- as counter ion in the lattice. The basal planes of the square-antiprism are constructed by O1, N13, N7, N12 and O2, N6, N1, N14 (Figure 4a). Ligands 2-methyl-8-quinolinol are almost perpendicular to the ligand Lz, which is different with the reported complexes, $[\text{DyLz}_2(\text{o-vanillin})_2] \cdot \text{X} \cdot \text{solvent}$ ($\text{X} = \text{Br}^-, \text{NO}_3^-, \text{CF}_3\text{SO}_3^-$)¹³ and $[\text{DyLz}_2(\text{salicylaldehyde})_2] \cdot \text{X} \cdot \text{solvent}$ ($\text{X} = \text{OH}^-, \text{Cl}^-, \text{Br}^-$),²⁹ in which the two sorts of ligands are relatively parallel. The ϕ value, defined as the space angle between the two Lz ligands or two 2-methyl-8-quinolinol ligands, is relatively large (38.45°) for two Lz ligands (Figure 4b) and very small (2.59°) for two 2-methyl-8-quinolinol ligands (Figure S1). However, the $\pi \cdots \pi$ distance of 4.039 Å for two 2-methyl-8-quinolinol ligands is larger than the value of 3.433 Å for two Lz ligands, which means the very weak $\pi \cdots \pi$ stacking effects. The *SHAPE* 2.1 software reveals that Dy^{III} ion resides in the square-antiprismatic coordination geometry (D_{4d}) with *CshM* of 1.434 for **3Dy**, which is larger than those of **1Dy** and **2Dy** (Table S3). The Dy–N distances range from 2.511(4) to 2.587(4) Å, while the two Dy–O distances are 2.214(3) and 2.217(3) Å, respectively (Table S2). The angles α vary from 49.2° to 66.6° and the θ angle between two basal planes is 8.7° , indicating the larger deviation of the ideal D_{4d} symmetry, which is consistent with the *SHAPE* calculation. The $\angle \text{O1-Dy-O2}$ angle of 137.46° for **3Dy** is smaller than 140.46° for perfect D_{4d} geometry.³⁰ The shortest intermolecular Dy...Dy distance is 9.14 Å, here again suggesting the potential presence of intermolecular interactions.

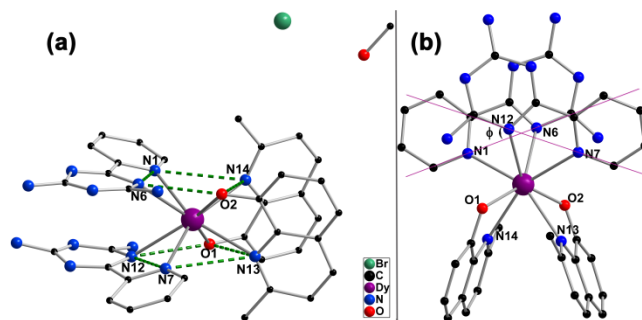


Figure 4. (a) Molecular structures of **3Dy**. (b) The solid lines represent the orientations of the two Lz ligands. H atoms are omitted for clarity.

Magnetic properties. Direct-current (dc) magnetic susceptibilities were studied for all three compounds under an applied field of 1 kOe from 2 to 300 K. As shown in Figure 5, the $\chi_M T$ values at room temperature of 14.29, 14.14, and 14.40 $\text{cm}^3 \text{K mol}^{-1}$ for **1Dy**, **2Dy** and **3Dy**, respectively, close to the expected value of 14.17 $\text{cm}^3 \text{K mol}^{-1}$ for Dy^{III} ion ($g = 4/3$ of the ${}^6H_{15/2}$ ground state of the Dy^{III} ion). For all three complexes, upon cooling, the $\chi_M T$ values remain constant in the range of 300–140 K, and then decrease slowly before a sharp drop below 8 K, reaching values of 11.06, 12.22 and 12.57 $\text{cm}^3 \text{K mol}^{-1}$ at 1.9 K for **1Dy**, **2Dy** and **3Dy**, respectively. The slow decrease can be attributed to the depopulation of stark sublevel, and the sharp decrease may arise from non-negligible intermolecular interactions between the Dy^{III} ions. The magnetization data (Figures S2–S4) of all three complexes show a steep increase in the range of 0–10 kOe field and then reach 6.52, 6.24 and 5.99 μ_B , respectively, at 1.9 K and 7 kOe. In addition, the non-superimposition of the M vs. H/T plots (Figures S2–S4, Inset) suggests the presence of significant magnetic anisotropy and/or low-lying excited states.

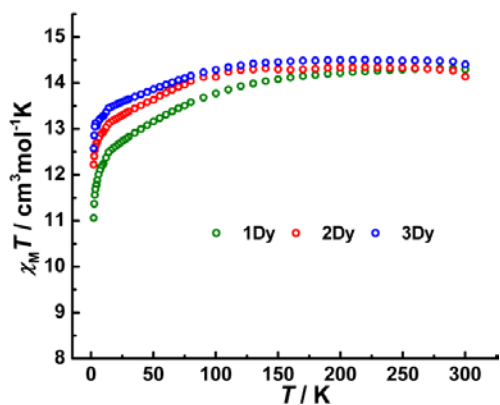


Figure 5. Plots of the $\chi_M T$ versus T for **1Dy** (green), **2Dy** (red) and **3Dy** (blue) in an applied field of 1 kOe.

The ac susceptibility measurements were performed on three complexes in zero applied dc field to probe the dynamics of the magnetization. Both the in-phase (χ') and out-of-phase (χ'') susceptibilities display a frequency (Figure 6) and temperature (Figures S5–S7) dependence for three complexes. Frequency-dependent out-of-phase (χ'') susceptibilities signals show that the peak maxima shift to a lower frequency when lowering the temperature, and then the frequency-independent regimes are observed for all three complexes, which could be attributed to quantum tunneling relaxation effects at zero dc field. Besides, the temperature-dependent magnetic susceptibility data show a rapid increase of χ'' signals in the low temperature region, which are coincident with the χ'' vs ν plots. The Cole-Cole plots (Figure S8) exhibit semi-circular shape which can be fitted to the generalized Debye model, giving α values in the ranges of 0.11–0.19, 0.01–0.15, and 0.02–0.11 for **1Dy**, **2Dy**, and **3Dy**, respectively, indicating a relatively small distributions of relaxation times.

The magnetization relaxation times τ obtained by fitting $\chi''(\nu)$ plots are plotted as a function of $1/T$ in Figure 7. In the high-temperature regime, Arrhenius analyses of the dynamic susceptibilities give Orbach process. However, the low temperature regimes become temperature-independent, characteristic of the QTM process. The intermediate regime may be dominated by Raman processes. In order to understand the whole relaxation mechanisms, a combination of relaxation processes has to be taken into account and then fitted the τ vs $1/T$ plots in the entire temperature range using the equation³¹

$$\tau_{obs}^{-1} = \tau_{QTM}^{-1} + CT^n + \tau_0^{-1} \exp\left(\frac{-U_{eff}}{T}\right)$$

Where the first and second terms account for quantum tunneling, and Raman processes, respectively, the third term represents the Orbach relaxation process. It's noteworthy that the direct process is not considered because the corresponding contribution is nullified in the zero dc field. The best fits gave parameters of $U_{eff} = 22 \text{ cm}^{-1}$ (32 K), $\tau_0 = 5.55 \times 10^{-5} \text{ s}$ (**1Dy**); $U_{eff} = 112 \text{ cm}^{-1}$ (162 K), $\tau_0 = 4.38 \times 10^{-6} \text{ s}$ (**2Dy**); $U_{eff} = 56 \text{ cm}^{-1}$ (80 K), $\tau_0 = 1.25 \times 10^{-5} \text{ s}$ (**3Dy**). The other parameters obtained from the fitting are shown in Table S4. Remarkably, butterfly-shaped magnetic hysteresis (Figure 7) in **1Dy** and **3Dy** are observed with a time-averaged sweep rate of 2.3 mT s^{-1} . While complex **2Dy** with highest effective energy barrier shows no hysteresis loop at 1.9 K, which may be attributed to the complication of the relaxations due to the presence of two crystallographically different molecules in one asymmetric unit.³²

Magnetic properties are sensitive to subtle differences in the coordination environment. Though all complexes presented herein show similar local D_{4d} coordination geometry, the magnetic relaxation barriers of the three complexes vary dramatically. The effective barrier of **1Dy** was extracted to be only 22 cm^{-1} , which is far less than that of **2Dy**. Contrary to the acac ligand, the TTA ligand having strong electron-withdrawing fluorine groups is probably a key factor to reduce the SMMs behavior of **1Dy**. For complex **3Dy**, the 2-methyl-8-quinolino ligands are almost perpendicular to the basal planes, which results in the large deviation from the ideal D_{4d} symmetry in the first coordination sphere compared with complex **2Dy**. Besides, the weak $\pi \cdots \pi$ stacking between the ligands may introduce transversal components as a result of the change of the electronic structure and coordination geometry.³⁰ Those two reasons mentioned above for complex **3Dy** lead to the fast QTM at low-temperature regions. Theoretical analyses were performed in order to understand this difference.

Theoretical analysis. The inherent large magnetic anisotropy and crystal field splitting of lanthanide complexes have attracted the attention of many researchers on single ion magnets.³³ However, compared with polynuclear SMMs based on TM ions, the relaxation of magnetization of SIMs is quite complicated due to the existence of several possible processes including Orbach, Raman, direct as well as QTM.^{33–34} Therefore, besides large crystal field splitting, other features in the aspect of electronic structure, which facilitate the suppression of unwanted fast relaxation, need to be achieved too.^{34–35} The most important fast relaxation is the QTM of which the rate scales as the square of the tunnel splitting Δ_{tun} . Clearly the effective suppression of QTM is the necessary condition for the observation of SMM behavior. Due to the time-reversal symmetry,³⁶ the microstates of Kramers systems, e.g., Dy^{III} ion, will be grouped into various degenerate doublets (KD) $|\pm n\rangle$ and the tunnel splitting Δ_{tun} could not exist for a KD under the

condition of strictly zero magnetic field.³⁶ However, small internal field actually exists in the real world and its transversal components, i.e., $H_{X,Y}$, will create Δ_{tun} via Zeeman interaction (eqn. 1a) with the corresponding magnetic moment of the KD,^{34,37} i.e., $\mu_{X,Y}$ (eqn. 1b).

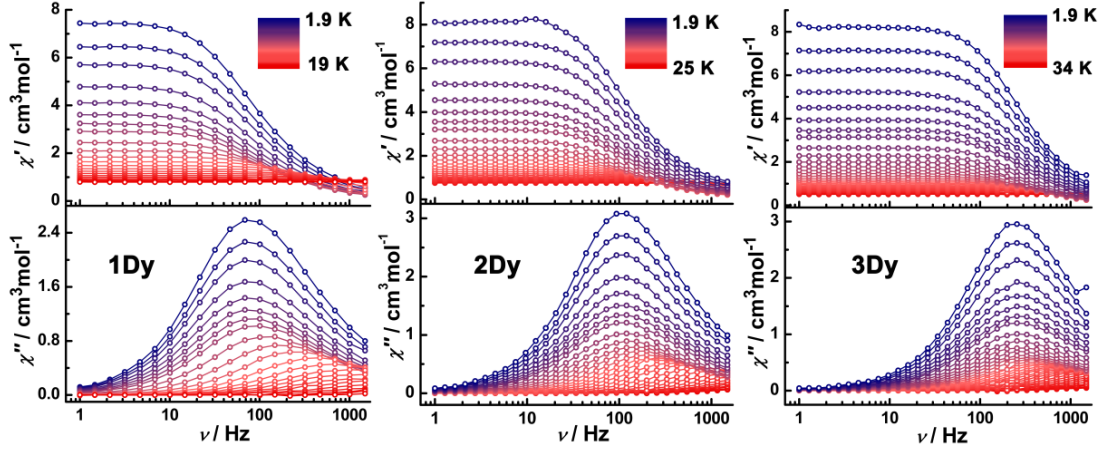


Figure 6. Frequency-dependent of χ' and χ'' ac susceptibility data for **1Dy** (left), **2Dy** (middle), and **3Dy** (right) under a zero dc field.

$$\Delta_{\text{tun}} = \left[(\mu_X H_X)^2 + (\mu_Y H_Y)^2 \right]^{1/2} \\ = \frac{1}{2} \left[\mu_B (g_X^2 H_X^2 + g_Y^2 H_Y^2) \right]^{1/2} \quad (1a)$$

$$\mu_\alpha = -\langle -n | \mu_B g_\alpha \hat{S}_\alpha | n \rangle = -\frac{1}{2} g_\alpha \mu_B \quad \alpha = X, Y, Z \quad (1b)$$

$$g_\alpha = 2 \langle -n | \mu_\alpha | n \rangle / \mu_B \quad \alpha = X, Y, Z \quad (1c)$$

The three main values ($g_{X,Y,Z}$) of the effective g factor of each KD are related with the components of the magnetic moment along various directions (eqn. 1b-1c). Clearly, to effectively suppress QTM, the parameter g_{XY} ^{15b} (eqn. 2a) should be as small as possible. Besides g_{XY} , *ab initio* calculations also provide μ_{QTM} (eqn. 2b), which could be used to estimate the strength of QTM too.

$$g_{XY} = (g_X^2 + g_Y^2)^{1/2} \quad (2a)$$

$$\mu_{\text{QTM}} = 1/3 (|\mu_x| + |\mu_y| + |\mu_z|) \quad (2b)$$

As listed in Table S5, the calculated g_Z values for the ground KD_0 approach the Ising limit of 20, verifying the easy-axis type of magnetic anisotropy. All the g_{XY} values of the KD_0 here are smaller than 0.015 which has been suggested to be a criterion for zero-field Dy^{III} -SIM.^{15b} Thus *ab initio* results are consistent with the appearance of SMM behavior of all the compounds here without the application of external dc field. However, when compared with recent reports on Dy^{III} -based SIMs of U_{eff} higher than 1000 K, the g_{XY} values here are higher than previous results ($0.8 \times 10^{-03} \sim 0.5 \times 10^{-05}$) by at least two orders of magnitude.^{4b, 38} Thus, it could be theoretically predicted that, although effectively suppressed to allow the observation of zero-field SMM behavior, residual QTM still exists for all the compounds here. This implication is experimentally echoed by the existence of rising tail in the imaginary part of the temperature dependence of the ac susceptibility (Figures S5-S7). Due to the existence of residual QTM as a live shortcut through the ground state, the possibility of mag-

netic relaxation via KDs higher than the first excited one (KD_1) should be negligible and thus the experimentally determined U_{eff} is clearly lower than the theoretical energy of KD_1 (Tables S4-S5).

As shown in Table S5, the QTM of **2Dy** should be weaker than those of **1Dy** and **3Dy** since **2Dy** has the smallest g_{XY} and μ_{QTM} . This is in accord with the fact that the variance between the experimental U_{eff} of **2Dy** (112 cm^{-1}) and theoretical energy of KD_1 (158.05 cm^{-1}) is the smallest one among all three compounds. Although **3Dy** attains the largest crystal field splitting as its energy of KD_1 (238.41 cm^{-1}) is the highest, the existence of QTM stronger than that of **2Dy** leads to the lower value of the fitted U_{eff} (56 cm^{-1}). It is not hard to understand the lowest U_{eff} of **1Dy** (22 cm^{-1}) since it has the strongest residual QTM as evidenced by the largest value of g_{XY} and μ_{QTM} .

Although possessing similar first coordination sphere, both g_{XY} and μ_{QTM} of **2Dy** are smaller than those of **1Dy** by one order of magnitude. Therefore significant difference in the aspect of electronic structure does exist and this should be the main reason for the fact that the experimental U_{eff} of **1Dy** is only one sixth of that of **2Dy**. Based on the theoretical orientation of the magnetic easy axis (Figure 8), the atoms of the first spheres of **1Dy** and **2Dy** can be classified into two groups: (1) the axial ones comprising of the four oxygen atoms lying close to the direction of easy axis and (2) the equatorial ones consisting of two nitrogen atoms and two oxygen atoms that approximately compose the equatorial plane assumed to be perpendicular to the easy axis.

Table 1. The results of the preliminary ESP (in a.u.) analysis on **1Dy** and **2Dy**.

	ratio ^a	ESP (ax)	ESP (equ)	Q (O_{ax}) ^b	Q (O_{equ}) ^b	Q (N_{equ}) ^b
1Dy	0.748	-1.129	-0.845	-0.712	-0.692	-0.421
2Dy	0.724	-1.164	-0.844	-0.730	-0.734	-0.378

^aESP(equ)/ESP(ax). ^bQ(O_{ax}) is the averaged charge of the four axial O atoms, Q(O_{equ}) is the averaged charge of the two equa-

torial O atoms and $Q(N_{\text{equ}})$ is the averaged charge of the two equatorial N atoms.

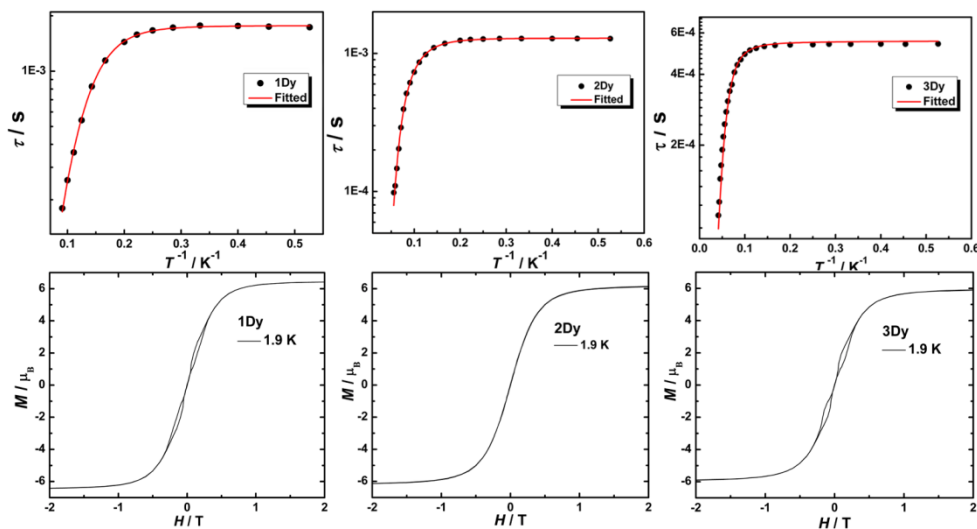


Figure 7. Plots of τ vs $1/T$ (top) and magnetic hysteresis loop (bottom) for **1Dy**, **2Dy**, and **3Dy**, respectively.

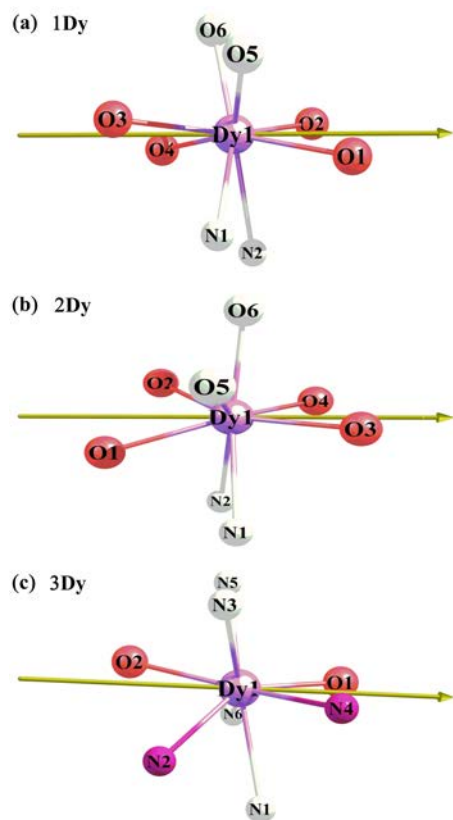


Figure 8. Orientation of the easy axis of the ground KD obtained from *ab initio* calculations for complexes **1Dy** (a), **2Dy** (b), and **3Dy** (c), respectively. (For the sake of clarity, only the first spheres are indicated and the equatorial atoms are shown in shade).

When only the eight atoms of the first sphere are included, the electrostatic potential (ESP) around the central Dy^{III} ion consists of two components: ESP(ax) which is the total contribution of the axial atoms and the collective contribution of the

equatorial atoms, denoted as ESP(equ). With the calculated atomic charges, both ESP(ax) and ESP(equ) could be estimated.

As seen from Table 1, the ratio of ESP(equ)/ESP(ax) is smaller than 1 for both **1Dy** and **2Dy**. This result indicates the excess of axial electrostatic repulsion around the central Dy^{III} ion over the equatorial one. Previous results on Dy^{III} -SIMs of both SAP³⁹ and other coordination geometries³⁵ have shown that this type of excess of axial repulsion will favor the electronic structure necessary for the ideal SMM properties. Thus the ESP analysis here is consistent with both the experimental observation and *ab initio* calculations. Furthermore, the ratio of **2Dy** (0.724) is clearly lower than that of **1Dy** (0.748) which implies the electronic structure of **2Dy** is closer to the ideal one. Once again, this result is in line with the experimental result of better SMM property of **2Dy** over that of **1Dy**.

Detailed analysis demonstrates that the better SMM property of **2Dy** over **1Dy** mainly arises from its larger magnitude of axial ESP (-1.164 a.u. vs -1.129 a.u.) since the ESP(equ) is nearly the same. In the aspect of structure, **1Dy** contains electron-withdrawing group, $-\text{CF}_3$, in the axial ligand providing the axial O atoms. As shown in Table 1, the $-\text{CF}_3$ group clearly depletes the magnitude of the negative charge of axial O atoms of **1Dy** (-0.712 a.u.) when compared with that of **2Dy** (-0.730 a.u.). Apparently, this reduction of the negative charge of axial O atoms, due to the introduction of electron-withdrawing group, accounts for the difference between **1Dy** and **2Dy** in the aspect of their magnetic properties. That is to say, the alternation of the O-donor ligands could induce significant impact on the Dy^{III} -SIM.

CONCLUSION

To summarize, using nitrogen-enriched ligand Lz here as auxiliary ligand, three mononuclear dysprosium complexes were synthesized through variation of the ligands with O donors. All complexes possess similar distorted molecular symmetry D_{4d} . However, subtle structural differences between the three complexes leads to different dynamic magnetic properties. The dynamic magnetic investigations show that all

complexes exhibit SMM behavior in a zero-dc field, while the effective magnetization relaxation barriers increased progressively from 22 cm⁻¹ (**1Dy**) to 56 cm⁻¹ (**3Dy**) and 112 cm⁻¹ (**2Dy**). These distinct magnetic properties can be attributed to two main factors: (1) the introduction of fluorine atoms in **1Dy** generated the strong electronic-withdrawing effects which reduce the magnetic axiality as verified by *ab initio* results; (2) the large deviation from the ideal D_{4d} symmetry geometry and the weak π···π stacking effects between ligands in **3Dy** induced the quantum tunneling of magnetizations in zero dc field. This work provides a means to modulate the magnetic properties of lanthanide-based SMMs with D_{4d} coordination geometry, highlighting the importance of electronic effect of ligands and the subtle changes of geometries.

ASSOCIATED CONTENT

Supporting Information.

Crystallographic data and selected bond lengths and angles (Tables S1–S2), SHAPE calculations (Table S3), parameters of Arrhenius Plot Fitting (Table S4), *Ab initio* results (Table S5), crystal structure (Figure S1), magnetic measurements (Figures S2–S8). CCDC 1513750 (**1Dy**), 1513751 (**2Dy**), 1513749 (**3Dy**) contain supplementary crystallographic data for this article. These data can be obtained free of charge from the Cambridge Crystallographic Data Centre via www.ccdc.cam.ac.uk/data_request/cif.

AUTHOR INFORMATION

Corresponding Author

*E-mail: tang@ciac.ac.cn

*E-mail: rayinyin@nwu.edu.cn

*E-mail: boris.leguennic@univ-rennes1.fr

Notes

The authors declare no competing financial interest.

ACKNOWLEDGMENT

We thank the National Natural Science Foundation of China (Grants 21525103, 21331003, 21521092 and 21103137) for financial support. B. L. G. thanks the French GENCI/IDRIS-CINES centers for high-performance computing resources.

REFERENCES

(1) (a)Tang, J.; Zhang, P. *Lanthanide Single Molecule Magnets*. Springer Berlin Heidelberg: Berlin, Heidelberg, 2015; (b)Layfield, R. A.; Murugesu, M. *Lanthanides and Actinides in Molecular Magnetism*. John Wiley & Sons: Weinheim, Germany: 2015; (c)Zhang, P.; Zhang, L.; Wang, C.; Xue, S.; Lin, S.-Y.; Tang, J. Equatorially Coordinated Lanthanide Single Ion Magnets. *J. Am. Chem. Soc.* **2014**, *136*, 4484-4487; (d)Meng, Y.-S.; Jiang, S.-D.; Wang, B.-W.; Gao, S. Understanding the Magnetic Anisotropy toward Single-Ion Magnets. *Acc. Chem. Res.* **2016**, *49*, 2381-2389; (e)Lu, J.; Guo, M.; Tang, J. Recent developments in lanthanide single-molecule magnets. *Chem. – Asian J.* **2017**, *12*, 2772-2779; (f)Woodruff, D. N.; Winpenny, R. E. P.; Layfield, R. A. Lanthanide Single-Molecule Magnets. *Chem. Rev.* **2013**, *113*, 5110-5148.

(2) (a)Freedman, D. E.; Harman, W. H.; Harris, T. D.; Long, G. J.; Chang, C. J.; Long, J. R. Slow Magnetic Relaxation in a High-Spin Iron(II) Complex. *J. Am. Chem. Soc.* **2010**, *132*, 1224-1225; (b)Harman, W. H.; Harris, T. D.; Freedman, D. E.; Fong, H.; Chang, A.; Rinehart, J. D.; Ozarowski, A.; Sougrati, M. T.; Grandjean, F.; Long, G. J.; Long, J. R.; Chang, C. J. Slow Magnetic Relaxation in a Family of Trigonal Pyramidal Iron(II) Pyrrolide Complexes. *J. Am. Chem. Soc.* **2010**, *132*, 18115-18126; (c)Kazin, P. E.; Zykin, M. A.; Trusov, L. A.; Eliseev, A. A.; Magdysyuk, O. V.; Dinnebie, R. E.; Kremer, R. K.; Felsler, C.; Jansen, M. A. Co-based single-molecule magnet confined in a barium phosphate apatite matrix

with a high energy barrier for magnetization relaxation. *Chem. Commun.* **2017**, *53*, 5416-5419; (d)Vallejo, J.; Pardo, E.; Viciano-Chumillas, M.; Castro, I.; Amoros del Torro, P.; Deniz, M.; Ruiz-Perez, C.; Yuste, C.; Krzystek, J.; Julve, M.; Lloret, F.; Cano, J. Reversible Solvatomagnetic Switching in a Single-Ion Magnet from an Entatic State. *Chem. Sci.* **2017**, *8*, 3694-3702.

(3) Zadrozny, J. M.; Xiao, D. J.; Atanasov, M.; Long, G. J.; Grandjean, F.; Neese, F.; Long, J. R. Magnetic Blocking in a Linear Iron(I) Complex. *Nat. Chem.* **2013**, *5*, 577-581.

(4) (a)Ishikawa, N.; Sugita, M.; Ishikawa, T.; Koshihara, S.-y.; Kaizu, Y. Lanthanide Double-Decker Complexes Functioning as Magnets at the Single-Molecular Level. *J. Am. Chem. Soc.* **2003**, *125*, 8694-8695; (b)Ding, Y.-S.; Chilton, N. F.; Winpenny, R. E. P.; Zheng, Y.-Z. On Approaching the Limit of Molecular Magnetic Anisotropy: A Near-Perfect Pentagonal Bipyramidal Dysprosium(III) Single-Molecule Magnet. *Angew. Chem. Int. Ed.* **2016**, *55*, 16071-16074; (c)Jiang, S.-D.; Wang, B.-W.; Sun, H.-L.; Wang, Z.-M.; Gao, S. An Organometallic Single-Ion Magnet. *J. Am. Chem. Soc.* **2011**, *133*, 4730-4733; (d)Brown, A. J.; Pinkowicz, D.; Saber, M. R.; Dunbar, K. R. A Trigonal-Pyramidal Erbium(III) Single-Molecule Magnet. *Angew. Chem. Int. Ed.* **2015**, *54*, 5864-5868; (e)Norel, L.; Darago, L. E.; Le Guennic, B.; Chakarawet, K.; Gonzalez, M. I.; Olshansky, J. H.; Rigaut, S.; Long, J. R. A Terminal Fluoride Ligand Generates Axial Magnetic Anisotropy in Dysprosium Complexes. *Angew. Chem. Int. Ed.* **2018**, *57*, 1933-1938.

(5) (a)Guo, F.-S.; Day, B. M.; Chen, Y.-C.; Tong, M.-L.; Mansikkamäki, A.; Layfield, R. A. A Dysprosium Metallocene Single-Molecule Magnet Functioning at the Axial Limit. *Angew. Chem. Int. Ed.* **2017**, *56*, 11445-11449; (b)Goodwin, C. A. P.; Ortu, F.; Reta, D.; Chilton, N. F.; Mills, D. P. Molecular Magnetic Hysteresis at 60 Kelvin in Dysprosocenium. *Nature* **2017**, *548*, 439-442.

(6) (a)Gatteschi, D.; Sessoli, R. Quantum Tunneling of Magnetization and Related Phenomena in Molecular Materials. *Angew. Chem. Int. Ed.* **2003**, *42*, 268-297; (b)AlDamen, M. A.; Clemente-Juan, J. M.; Coronado, E.; Martí-Gastaldo, C.; Gaita-Ariño, A. Mononuclear Lanthanide Single-Molecule Magnets Based on Polyoxometalates. *J. Am. Chem. Soc.* **2008**, *130*, 8874-8875; (c)Jiang, S.-D.; Wang, B.-W.; Su, G.; Wang, Z.-M.; Gao, S. A Mononuclear Dysprosium Complex Featuring Single-Molecule-Magnet Behavior. *Angew. Chem. Int. Ed.* **2010**, *49*, 7448-7451.

(7) (a)Dei, A.; Gatteschi, D. Molecular (Nano) Magnets as Test Grounds of Quantum Mechanics. *Angew. Chem. Int. Ed.* **2011**, *50*, 11852-11858; (b)Wäckerlin, C.; Donati, F.; Singha, A.; Baltic, R.; Rusponi, S.; Diller, K.; Patthey, F.; Pivetta, M.; Lan, Y.; Klyatskaya, S.; Ruben, M.; Brune, H.; Dreiser, J. Giant Hysteresis of Single-Molecule Magnets Adsorbed on a Nonmagnetic Insulator. *Adv. Mater.* **2016**, *28*, 5195-5199.

(8) Ungur, L.; Le Roy, J. J.; Korobkov, I.; Murugesu, M.; Chibotaru, L. F. Fine-tuning the Local Symmetry to Attain Record Blocking Temperature and Magnetic Remanence in a Single-Ion Magnet. *Angew. Chem. Int. Ed.* **2014**, *53*, 4413-4417.

(9) Guo, M.; Wang, Y.; Wu, J.; Zhao, L.; Tang, J. Structures and Magnetic Properties of Dysprosium Complexes: the Effect of Crystallization Temperature. *Dalton Trans.* **2017**, *46*, 564-570.

(10) (a)Habib, F.; Lin, P.-H.; Long, J.; Korobkov, I.; Wernsdorfer, W.; Murugesu, M. The Use of Magnetic Dilution To Elucidate the Slow Magnetic Relaxation Effects of a Dy^{III} Single-Molecule Magnet. *J. Am. Chem. Soc.* **2011**, *133*, 8830-8833; (b)Zhang, L.; Jung, J.; Zhang, P.; Guo, M.; Zhao, L.; Tang, J.; Le Guennic, B. Site-Resolved Two-Step Relaxation Process in an Asymmetric Dy^{III} Single-Molecule Magnet. *Chem. – Eur. J.* **2016**, *22*, 1392-1398; (c)da Cunha, T. T.; Jung, J.; Boulon, M.-E.; Campo, G.; Pointillart, F.; Pereira, C. L. M.; Le Guennic, B.; Cador, O.; Bernot, K.; Pineider, F.; Golhen, S.; Ouahab, L. Magnetic Poles Determinations and Robustness of Memory Effect upon Solubilization in a Dy^{III}-Based Single Ion Magnet. *J. Am. Chem. Soc.* **2013**, *135*, 16332-16335; (d)Pugh, T.; Chilton, N. F.; Layfield, R. A. Antimony-ligated dysprosium single-molecule magnets as catalysts for stibine dehydrocoupling. *Chem. Sci.* **2017**, *8*, 2073-2080.

(11) (a)Pointillart, F.; Bernot, K.; Golhen, S.; Le Guennic, B.; Guizouarn, T.; Ouahab, L.; Cador, O. Magnetic Memory in an Isotopically Enriched and Magnetically Isolated Mononuclear Dysprosium Complex. *Angew. Chem. Int. Ed.* **2015**, *54*, 1504-1507; (b)Huang, G.; Yi, X.; Jung, J.; Guillou, O.; Cador, O.; Pointillart, F.; Le Guennic, B.; Bernot, K. Optimization of Magnetic Relaxation and Isotopic Enrichment in Dimeric Dy^{III} Single-Molecule Magnets. *Eur. J. Inorg. Chem.* **2018**, *2018*, 326-332; (c)Kishi, Y.; Pointillart, F.; Lefeuvre, B.; Riobe, F.; Le Guennic, B.; Golhen, S.; Cador, O.; Maury, O.; Fujiwara, H.; Ouahab, L. Isotopically

- enriched polymorphs of dysprosium single molecule magnets. *Chem. Commun.* **2017**, *53*, 3575-3578.
- (12) (a) Rinehart, J. D.; Fang, M.; Evans, W. J.; Long, J. R. A N_2^{3-} Radical-Bridged Terbium Complex Exhibiting Magnetic Hysteresis at 14 K. *J. Am. Chem. Soc.* **2011**, *133*, 14236-14239; (b) Layfield, R. A.; McDouall, J. J. W.; Sulway, S. A.; Tuna, F.; Collison, D.; Wimpenny, R. E. P. Influence of the N-Bridging Ligand on Magnetic Relaxation in an Organometallic Dysprosium Single-Molecule Magnet. *Chem. – Eur. J.* **2010**, *16*, 4442-4446.
- (13) Wu, J.; Jung, J.; Zhang, P.; Zhang, H.; Tang, J.; Le Guennic, B. Cis-trans Isomerism Modulates the Magnetic Relaxation of Dysprosium Single-Molecule Magnets. *Chem. Sci.* **2016**, *7*, 3632-3639.
- (14) Liu, J.-L.; Chen, Y.-C.; Zheng, Y.-Z.; Lin, W.-Q.; Ungur, L.; Wernsdorfer, W.; Chibotaru, L. F.; Tong, M.-L. Switching the anisotropy barrier of a single-ion magnet by symmetry change from quasi- D_{5h} to quasi-Oh. *Chem. Sci.* **2013**, *4*, 3310-3316.
- (15) (a) Bernot, K.; Luzon, J.; Bogani, L.; Etienne, M.; Sangregorio, C.; Shanmugam, M.; Caneschi, A.; Sessoli, R.; Gatteschi, D. Magnetic Anisotropy of Dysprosium(III) in a Low-Symmetry Environment: A Theoretical and Experimental Investigation. *J. Am. Chem. Soc.* **2009**, *131*, 5573-5579; (b) Aravena, D.; Ruiz, E. Shedding Light on the Single-Molecule Magnet Behavior of Mononuclear Dy^{III} Complexes. *Inorg. Chem.* **2013**, *52*, 13770-13778; (c) Bi, Y.; Guo, Y.-N.; Zhao, L.; Guo, Y.; Lin, S.-Y.; Jiang, S.-D.; Tang, J.; Wang, B.-W.; Gao, S. Capping Ligand Perturbed Slow Magnetic Relaxation in Dysprosium Single-Ion Magnets. *Chem. – Eur. J.* **2011**, *17*, 12476-12481.
- (16) Chen, G.-J.; Guo, Y.-N.; Tian, J.-L.; Tang, J.; Gu, W.; Liu, X.; Yan, S.-P.; Cheng, P.; Liao, D.-Z. Enhancing Anisotropy Barriers of Dysprosium(III) Single-Ion Magnets. *Chem. – Eur. J.* **2012**, *18*, 2484-2487.
- (17) Guo, M.; Xu, Y.; Wu, J.; Zhao, L.; Tang, J. Geometry and magnetic interaction modulations in dinuclear Dy_2 single-molecule magnets. *Dalton Trans.* **2017**, *46*, 8252-8258.
- (18) Case, F. H.; Koft, E. The Synthesis of Certain Substituted 1,3,5-Triazines Containing the Ferriin Group. *J. Am. Chem. Soc.* **1959**, *81*, 905-906.
- (19) (a) Sheldrick, G. M. *SHELXS-97 Program for Crystal Structure Solution*. University of Göttingen: Germany: 1997; (b) Sheldrick, G. A short history of SHELX. *Acta Crystallogr. Sect. A* **2008**, *64*, 112-122; (c) Sheldrick, G. Crystal structure refinement with SHELXL. *Acta Crystallogr. Sect. C* **2015**, *71*, 3-8.
- (20) Bain, G. A.; Berry, J. F. Diamagnetic Corrections and Pascal's Constants. *J. Chem. Educ.* **2008**, *85*, 532.
- (21) Luzon, J.; Sessoli, R. Lanthanides in molecular magnetism: so fascinating, so challenging. *Dalton Trans.* **2012**, *41*, 13556-13567.
- (22) Roos, B. O.; Taylor, P. R.; Siegbahn, P. E. M. A Complete Active Space SCF Method (CASSCF) Using a Density Matrix Formulated Super-CI Approach. *Chem. Phys.* **1980**, *48*, 157-173.
- (23) Malmqvist, P. Å.; Roos, B. O.; Schimmelpfennig, B. The Restricted Active Space (RAS) State Interaction Approach with Spin-Orbit Coupling. *Chem. Phys. Lett.* **2002**, *357*, 230-240.
- (24) (a) Roos, B. O.; Lindh, R.; Malmqvist, P.-Å.; Veryazov, V.; Widmark, P.-O. Main Group Atoms and Dimers Studied with a New Relativistic ANO Basis Set. *J. Phys. Chem. A* **2004**, *108*, 2851-2858; (b) Roos, B. O.; Lindh, R.; Malmqvist, P.-Å.; Veryazov, V.; Widmark, P.-O. New Relativistic ANO Basis Sets for Transition Metal Atoms. *J. Phys. Chem. A* **2005**, *109*, 6575-6579.
- (25) (a) Chibotaru, L. F.; Ungur, L. Ab initio calculation of anisotropic magnetic properties of complexes. I. Unique definition of pseudospin Hamiltonians and their derivation. *J. Chem. Phys.* **2012**, *137*, 064112; (b) Chibotaru, L. F. In *Adv. Chem. Phys.*; John Wiley & Sons, Inc.: 2013; pp 397-519.
- (26) Aquilante, F.; Autschbach, J.; Carlson, R. K.; Chibotaru, L. F.; Decey, M. G.; De Vico, L.; Fdez. Galván, I.; Ferré, N.; Frutos, L. M.; Gagliardi, L.; Garavelli, M.; Giussani, A.; Hoyer, C. E.; Li Manni, G.; Lischka, H.; Ma, D.; Malmqvist, P. Å.; Müller, T.; Nenov, A.; Olivucci, M.; Pedersen, T. B.; Peng, D.; Plasser, F.; Pritchard, B.; Reiher, M.; Rivalta, I.; Schapiro, I.; Segarra-Martí, J.; Stenrup, M.; Truhlar, D. G.; Ungur, L.; Valentini, A.; Vancoillie, S.; Veryazov, V.; Vysotskiy, V. P.; Weingart, O.; Zapata, F.; Lindh, R. Molcas 8: New capabilities for multiconfigurational quantum chemical calculations across the periodic table. *J. Comput. Chem.* **2016**, *37*, 506-541.
- (27) Ruiz-Martínez, A.; Casanova, D.; Alvarez, S. Polyhedral Structures with an Odd Number of Vertices: Nine-Coordinate Metal Compounds. *Chem. – Eur. J.* **2008**, *14*, 1291-1303.
- (28) Sorace, L.; Benelli, C.; Gatteschi, D. Lanthanides in molecular magnetism: old tools in a new field. *Chem. Soc. Rev.* **2011**, *40*, 3092-3104.
- (29) Wu, J.; Li, X.-L.; Zhao, L.; Guo, M.; Tang, J. Enhancement of Magnetocaloric Effect through Fixation of Carbon Dioxide: Molecular Assembly from Ln_4 to Ln_4 Cluster Pairs. *Inorg. Chem.* **2017**, *56*, 4104-4111.
- (30) Wu, J.; Cador, O.; Li, X.-L.; Zhao, L.; Le Guennic, B.; Tang, J. Axial Ligand Field in D_{4d} Coordination Symmetry: Magnetic Relaxation of Dy SMMs Perturbed by Counteranions. *Inorg. Chem.* **2017**, *56*, 11211-11219.
- (31) (a) Benelli, C.; Gatteschi, D. *Introduction to molecular magnetism: From transition metals to lanthanides*. John Wiley & Sons: Weinheim, Germany: 2015; (b) Demir, S.; Zadrozny, J. M.; Long, J. R. Large Spin-Relaxation Barriers for the Low-Symmetry Organolanthanide Complexes $[Cp^*_2Ln(BPh_4)]$ (Cp^* =pentamethylcyclopentadienyl; $Ln=Tb, Dy$). *Chem. – Eur. J.* **2014**, *20*, 9524-9529; (c) Long, J.; Shestakov, B. G.; Liu, D.; Chibotaru, L. F.; Guari, Y.; Cherkasov, A. V.; Fukin, G. K.; Trifonov, A. A.; Larionova, J. An Organolanthanide(III) Single-Molecule Magnet with an Axial Crystal-Field: Influence of the Raman Process over the Slow Relaxation. *Chem. Commun.* **2017**, *53*, 4706-4709.
- (32) Yao, X.-N.; Du, J.-Z.; Zhang, Y.-Q.; Leng, X.-B.; Yang, M.-W.; Jiang, S.-D.; Wang, Z.-X.; Ouyang, Z.-W.; Deng, L.; Wang, B.-W.; Gao, S. Two-Coordinate Co(II) Imido Complexes as Outstanding Single-Molecule Magnets. *J. Am. Chem. Soc.* **2017**, *139*, 373-380.
- (33) Liddle, S. T.; van Slageren, J. Improving f-element Single Molecule Magnets. *Chem. Soc. Rev.* **2015**, *44*, 6655-6669.
- (34) Ungur, L.; Chibotaru, L. F. Strategies toward High-Temperature Lanthanide-Based Single-Molecule Magnets. *Inorg. Chem.* **2016**, *55*, 10043-10056.
- (35) Li, M.; Wu, H.; Yang, Q.; Ke, H.; Yin, B.; Shi, Q.; Wang, W.; Wei, Q.; Xie, G.; Chen, S. Experimental and Theoretical Interpretation on the Magnetic Behavior in a Series of Pentagonal-Bipyramidal Dy^{III} Single-Ion Magnets. *Chem. – Eur. J.* **2017**, *23*, 17775-17787.
- (36) Abragam, A.; Bleaney, B. *Electron Paramagnetic Resonance of Transition Ions*. Clarendon Press: Oxford, 1970.
- (37) Chibotaru, L. F. In *Molecular Nanomagnets and Related Phenomena*; Gao, S., Ed.; Springer Berlin Heidelberg: Berlin, Heidelberg, 2015; Vol. 164, pp 185-229.
- (38) Liu, J.; Chen, Y.-C.; Liu, J.-L.; Vieru, V.; Ungur, L.; Jia, J.-H.; Chibotaru, L. F.; Lan, Y.; Wernsdorfer, W.; Gao, S.; Chen, X.-M.; Tong, M.-L. A Stable Pentagonal Bipyramidal $Dy(II)$ Single-Ion Magnet with a Record Magnetization Reversal Barrier over 1000 K. *J. Am. Chem. Soc.* **2016**, *138*, 5441-5450.
- (39) Zhang, S.; Wu, H.; Sun, L.; Ke, H.; Chen, S.; Yin, B.; Wei, Q.; Yang, D.; Gao, S. Ligand Field Fine-tuning on the Modulation of the Magnetic Properties and Relaxation Dynamics of Dysprosium(III) Single-Ion Magnets (SIMs): synthesis, structure, magnetism and Ab Initio Calculations. *J. Mater. Chem. C* **2017**, *5*, 1369-1382.

SYNOPSIS TOC

Manipulation of the magnetic relaxation was demonstrated in a series of mononuclear Dy^{III} complexes with the same auxiliary ligand Lz through alteration of the ligands containing O donors.

